Research paper

Fabrication of TiO$_2$ hollow microspheres assembly from nanosheets (TiO$_2$-HMSs-NSs) with enhanced photoelectric conversion efficiency in DSSCs and photocatalytic activity

Ruiwen Yang [a], Jinghua Cai [a], Kangle Lv [a,*], Xiaofeng Wu [a], Wenguang Wang [b], Zhihua Xu [c], Mei Li [a,*], Qin Li [a], Weiqing Xu [d]

[a] *Key Laboratory of Catalysis and Materials Science of the State Ethnic Affairs Commission and Ministry of Education, Hubei Province, College of Resources and Environmental Science, South-Central University for Nationalities, Wuhan 430074, PR China*
[b] *School of Materials and Energy, Guangdong University of Technology, Guangzhou 510006, PR China*
[c] *Key Laboratory of Optoelectronic Chemical Materials and Devices of Ministry of Education, Flexible Display Materials and Technology Co-Innovation Centre of Hubei Province, Jianghan University, Wuhan 430056, PR China*
[d] *State Key Laboratory of Supramolecular Structure and Materials, Jilin University, Changchun 130012, PR China*

ABSTRACT

Fabrication of TiO$_2$ hollow microspheres (TiO$_2$-HMSs) with complex structure is of great importance but remains a great challenge. In this paper, hierarchical TiO$_2$ hollow microspheres assembly from nanosheets (TiO$_2$-HMSs-NSs) were prepared by hydrothermal treatment of TiO$_2$-HMSs precursor in NaOH solution and followed by acid wash and calcination. The effect of hydrothermal reaction time on the structure and photoelectric conversion performances of TiO$_2$-HMSs-NSs film solar cells was systematically studied. It was found that both the BET surface area and photocatalytic activity of TiO$_2$-HMSs-NSs, in photocatalytic degradation of Brilliant Red X-3B dye, are positively related to the hydrothermal reaction time (from 0 to 3 h). The BET specific area of TiO$_2$-HMSs-NSs steady increase from 21 m^2 g^{-1} of TiO$_2$-HMSs precursor (H0) to 184 m^2 g^{-1} (H3), improved by a factor of 8.76, while the photocatalytic activity of H3 increased 7.50 times when compared with that of H0 sample. The highest photoelectric conversion efficiency (5.97%) of TiO$_2$-HMSs-NSs film solar cell was obtained for H2 sample, exceeding that of TiO$_2$-HMSs precursor (H0) based film solar cell (3.75%) with the same film thickness by a factor of 1.6. The improved photoelectric conversion efficiency of TiO$_2$-HMSs-NSs based solar cell was attributed to the unique hierarchical hollow structure, which results in a good contact between TiO$_2$ and FTO glass, enlarged pore volume, enhanced adsorption to sensitizer and improved light scattering ability.

© 2017 Elsevier B.V. All rights reserved.

1. Introduction

In recent years, dye-sensitized solar cells (DSSCs) have attracted much attention due to their low cost and the possibility to fabricate flexible solar cells, which is regarded as one of the most promising alternatives to the traditional silicon solar cell [1,2]. The structure of DSSCs contains the following three parts [3]: (1) TiO$_2$ film photoanode, which has adsorbed sensitizer dye and is deposited on a transparent conducting glass, (2) electrolyte solution, which is penetrating throughout the porous TiO$_2$ film, and (3) the counter electrode, which is a piece of platinized transparent conducting oxide glass.

TiO$_2$ is considered as the most suitable materials for widespread solar energy conversion and environmental applications due to its biological and chemical inertness, strong oxidizing power, cost effectiveness, long-term stability against photocorrosion and chemical corrosion [3,4]. It was reported that the morphology, porous structure, exposed facets and crystallinity of TiO$_2$ play important roles in the photoelectric conversion efficiency of DSSCs [3,5]. Up to now, TiO$_2$ nanomaterials with different morphologies such as nanoparticles [6], nanotubes [7], nanowires [8], nanofibers [9], nanobelts [10], nanosheets [11] and microspheres [12,13], have been used to fabricate photoanode film of DSSCs. It is generally accepted that high specific surface area and excellent light scattering property are benificial to the improvement of the photoelectric conversion efficiency of the DSSCs. Unfortunately, these factors are

always incompatible with one another. It has been reported that [3], smaller TiO_2 nanoparticles (in sizes of 10–20 nm as an example) possess large specific surface area, which is beneficialfor loading abundant dye molecules. However, these TiO_2 nanoparticles film is transparent with poor light harvesting due to the particle size is smaller than the wavelength of visible light. On the contrary, TiO_2 film with larger particles (100–400 nm) favors for the effective light scattering, but the smaller surface area resulting in poor dye adsorption capacity.

To solve the problems mentioned above, multi-layered and even graded photoanode films consisting of TiO_2 nanostructures with different sizes or morphologies have been studied, which is expected to accommodate their specific advantages. For example, Zhao et al. reported the preparation of TiO_2-HMSs/nanorod array [14] and TiO_2 nanotubes/nanoparticles [15,16] double-layer film, and even TiO_2 nanoparticles/nanotubes array/hollow nanoboxes [17] three-layer film photoanode based DSSCs, which showed improved photoelectric conversion efficiency. Recently, Marimuthu et al. [18] reported the preparation of ZnO nanowire arrays and nanoneedle arrays decorated TiO_2 film DSSCs, and Wang et al. [5] fabricated a TiO_2 film photoanode with nanosheet/nanoparticle gradient structure, and the enhanced photoelectric conversion performance was attributed to the strong light scattering ability of the gradient structure and good electronic contact between the TiO_2 nanoparticle underlayer and FTO glass. However, the procedure for the fabrication of these photoanode films with multi-components is complex and time-consuming. Therefore, method on facile fabrication of TiO_2 films photoanode possessing high photoelectric conversion efficiency in DSSCs is urgently needed but remains a great challenge.

On considering that hierarchical nanomaterials have the merits of large surface areas for abundant dye sensitizer adsorption and hollow (porous) structures for light scattering, both the goals of improvement on sensitizer adsorption and light scattering can be achieved by fabrication of single component hierarchical structured TiO_2 film based DSSCs. Here we prepared hierarchical TiO_2 hollow microspheres assembly from nanosheets (TiO_2-HMSs-NSs) by hydrothermal treatment of primary TiO_2 hollow microspheres (TiO_2-HMSs) in NaOH solution, and followed by acid wash and calcination. Using this strategy, TiO_2 nanoparticles can transform into nanosheets, sharply increase the BET surface areas. The structure of TiO_2-HMSs-NSs was tailored by control the hydrothermal reaction time. We therefore systematically studied the relationship between microstructure and photoelectric conversion efficiency of TiO_2-HMSs-NSs film based DSSCs.

To the best of our knowledge, it is the first time to report the one-step fabrication of the hierarchically structured TiO_2-HMSs-NSs film based DSSCs. The difunctionality of TiO_2-HMSs-NSs makes this DSSCs possess the advantages of multi-layered or gradient structure film photoanode based DSSCs.

2. Experimental

2.1. Preparation of primary TiO_2 hollow microspheres

Primary TiO_2 hollow microspheres (TiO_2-HMSs) precursor was prepared according to our previous report [19]. In a typical synthesis, 2.42 g of urea (40 mmol) was added into 65 mL of $(NH_4)_2TiF_6$ solution (1.19 g, 6 mmol) under vigorous stirring. Then, 15 mL of H_2O_2 (30 wt.%) was dropwise added into the mixed solution, which was transferred to a 100 mL Teflon-lined autoclave and sealed. After kept at 200 °C for 10 h, the obtained precipitate was filtrated and washed by distilled water until the pH value of the filtrate is about 7.

Table 1
Physical property of the photocatalyst.

Samples	Precursor	Reaction time (h)	Characterization results		
			S_{BET} (m^2 g^{-1})	PV (cm^3 g^{-1})	APS (nm)
H0	TiO_2-HMS	0	21	0.11	18.6
H1	TiO_2-HMS	1	30	0.19	21.9
H1.5	TiO_2-HMS	1.5	51	0.31	19.3
H2	TiO_2-HMS	2	154	0.63	13.0
H2.5	TiO_2-HMS	2.5	174	0.69	12.2
H3	TiO_2-HMS	3	184	0.70	11.8
S3	TiO_2-SMS	3	73	0.36	13.7

For comparison, TiO_2 solid microspheres (TiO_2-SMSs) were also prepared under other identical conditions except in the presence of 1 mL of H_2O_2 and 79 mL of aqueous solution.

2.2. Preparation of TiO_2 hollow microspheres assembly from nanosheets

Hierarchical TiO_2 hollow microspheres assembly from nanosheets (TiO_2-HMSs-NSs) were synthesized by hydrothermal treatment of TiO_2-HMSs precursor in basic solution. Similar strategy has been reported in the literature [20]. Typically, precursor TiO_2-HMSs (0.5 g) are dispersed in 50 mL of 10 M NaOH solution, which is followed by hydrothermal treatment at 120 °C for 3 h in a Teflon autoclave. The resulted precipitates were redispersed into 600 mL of HCl solution (0.1 M) under magnetic stirring for 12 h. After washed thoroughly with distilled water until the pH value of the filtrate is about 7, the powder was further calcined at 400 °C for 1 h to obtained the product (H3 sample).

Similarly, a serial of samples were prepared under other identical conditions except the difference in hydrothermal reaction time. The prepared TiO_2-HMSs-NSs is labeled as Hx, where "x" represents the hydrothermal reaction time (Table 1). Note that sample H0 represents the precursor TiO_2-HMSs.

For a comparative study, the experiment was also carried out using TiO_2-SMSs as the precursor under identical condition as that of H3 sample, and the product is labeled as S3 (hydrothermal reaction in NaOH solution for 3 h).

2.3. Fabrication of DSSCs substance

TiO_2-HMSs-NSs was pasted onto the FTO glass (Nippon sheet glass, 14–20 Ω per square) by a screen printing method technique as our reported before [5]. After drying in air for 10 min, the film was heated in oven at 80 °C for 10 min to evaporate the organic solvent. After carried out the repeated printing to get 10 layers, the film was calcined in a tubular muffle furnace at 450 °C for 30 min to remove the organics.

After cool down to room temperature, TiO_2 films were immersed in anhydrous ethanol solution containing 0.5 mM of N719 dye (Hepta Chroma Solar Tech, Dalian, China) for 24 h for adsorption of dye (sensitizer). Afterwards, the dye-sensitized films were rinsed with ethanol to remove physical-adsorbed N719 dye molecules. Finally, the obtained TiO_2 film electrodes were dried in an oven at 80 °C for 2 h.

The sensitized photoanode were clamped together with Pt counter electrode, and the mixed solution of 0.5 M LiI, 0.05 M I_2, 0.5 M 4-tertbutylpyridine, and 0.3 M 1,2-dimethyl-3-propylimidazolium iodide (DMPII) in dry acetonitrile was used as electrolyte. The assembled cell was tested immediately.

2.4. Characterization

The X-ray diffraction (XRD) patterns obtained on a D8-advance X-ray diffractometer (German Bruker). The accelerated voltage and applied current were 15 kV and 20 mA, respectively. The morphology of TiO_2 powders was observed on a transmission electron microscope (TEM) (Tecnai G20, USA) using an acceleration voltage of 200 kV and a field emission scanning electron microscope (FESEM) (S-4800, Hitachi, Japan) with an acceleration voltage of 10 kV, respectively. Nitrogen adsorption–desorption isotherms were obtained on an ASAP 2020 (Micromeritic Instruments, USA) nitrogen adsorption apparatus. All the samples were degassed at 120 °C prior to Brunauer–Emmett–Teller (BET) measurements. The BET specific surface area (S_{BET}) was determined by a multipoint BET method using the adsorption data in the relative pressure P/P_0 range of 0.05–0.30. The desorption isotherm was used to determine the pore size distribution by using the Barret-Joyner-Halenda (BJH) method. The nitrogen adsorption volume at $P/P_0 = 0.994$ was used to determine the pore volume (PV) and average pore size (APS). UV–vis diffuse reflectance spectra (DRS) were obtained on a UV–vis spectrophotometer (LambdaBio35) using $BaSO_4$ as the reference. A solar simulator (Newport 91160) with an intensity of 100 mW cm^{-2} (1 sun) was employed as the light resource. The active area of DSSCs was 0.14 cm^2. The impedance parameters were obtained by fitting the equivalent circuit of Nyquist graph using Z-view software.

2.5. Photocatalytic degradation of organic dye

A 3 W LED lamp (UVEC-4 II, Shenzhen lamplic, China) emitted mainly at 365 nm is used as light source, which is placed outside a Pyrex-glass reactor at a fixed distance (ca. 5 cm). Brilliant Red X-3B (X3B), an anionic azo dye, is used as a probe molecule. During the photocatalytic reaction, the reactor was mechanically stirred at a constant rate. The concentration of TiO_2 was 1.0 g L^{-1}, and the initial concentration of X3B was 1.0×10^{-4} mol L^{-1}. Before irradiation, the suspensions were sonicated for 5 min, which were then shaken overnight in the dark to establish the adsorption-desorption equilibrium. At given intervals of irradiation, small aliquots were withdrawn by a syringe, and filtered through a membrane (pore size 0.45 μm). The concentration of X3B remaining in the filtrate was then analyzed by an Agilent 8451 spectrometer at 530 nm.
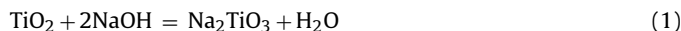
3. Results and discussion

3.1. Morphology evolution and phase structure

Fig. 1 presents the shape evolution of TiO_2-HMSs-NSs (H2 sample as an example) at different reaction stage. Before reaction, it can be seen that the diameters of the precursor TiO_2-HMSs are in the range of 0.8-1.0 um (Fig. 1a). Enlarged TEM image shows that TiO_2-HMSs have rough surface, which are produced through self-assembly of TiO_2 nanoparticles. A sharp peak at $2\theta = 25.3°$, corresponding to the (101) plane diffraction of anatase TiO_2 (JCPDS No. 21-1272) [21], was observed for the XRD pattern of TiO_2-HMSs precursor (Fig. 2a), indicating that well crystallized anatase TiO_2-HMSs precursor was successfully synthesized [19].

After hydrothermal treatment in NaOH solution at 120 °C for 2 h, and followed by acid-wash, hierarchical hollow microspheres with similar diameters of TiO_2-HMSs precursor were produced (Fig. 1b). However, careful view shows that the surface of the hollow microspheres are covered with multi-layered nanosheets, and some of the nanosheets converted into nanotubes, either by scrolling (rolling-up) single layer nanosheets or by curving (wrapping) of conjoined nanosheets, forming urchin-like hollow structures. At this stage, XRD characterization result reflects that the main peak at $2\theta = 25.3°$, corresponding to the (101) plane diffraction of anatase TiO_2, disappeared, which is possibly due to the phase transformation from anatase TiO_2 to sodium titanate (comparing Fig. 2a and b). It has been well documented that sodium titanate nanosheets can be obtained by hydrothermal treatment the mixed solution of P25 TiO_2 and NaOH to form Na_2TiO_3 (Eq. (1)), which can further transform to hydrogen titanate (Eq. (2)) after acid wash, and then to anatase TiO_2 (Eq. (3)) by calcination [22,23].

$$TiO_2 + 2NaOH = Na_2TiO_3 + H_2O \qquad (1)$$

$$Na_2TiO_3 + 2HCl = H_2TiO_3 + 2NaCl \qquad (2)$$

$$H_2TiO_3 + heat = TiO_2 + H_2O \qquad (3)$$

Therefore, the rough surface of hollow microspheres shown in Fig. 1b is actually formed due to the curving (wrapping) of conjoined nanosheets. Although calcination results in the phase transformation from hydrogen titanate nanosheets to anatase TiO_2 nanosheets (Fig. 2b and c), heat treatment has little effect on the morphology of titanate hollow microspheres (Fig. 1b and c).

To get more information on the formation of TiO_2-HMSs-NSs, the growth process of H3 sample was followed by examining the products at different intervals of hydrothermal reaction time. According to the TEM images, after reaction for 1 h, the morphology of the TiO_2-HMSs precursor almost keeps unchanged (Figs. 1 a and 3 a). However, nanosheets in small sizes were observed covering on the surface of TiO_2-HMSs (SEM image in Fig. 4a). The nanosheets should be sodium titanate due to the reaction between TiO_2 nanoparticle and NaOH (Eq. (1)). With extension the reaction time to 1.5 h, the density of the formed titanate nanosheets sharply increased (Figs. 3 b and 4 b), resulting in the decrease in diameter of the cavity. When further increase in the reaction time to 2 h (Figs. 1 b and 4 c) and 2.5 h (Figs. 3 c and 4 d), the hollow interiors becomes smaller and smaller because of the over growth of titanate nanosheets. After reaction for 3 h, the hollow interiors of the precursor can hardly be seen both from the TEM (Fig. 3d) and SEM image (Fig. 4e). At this stage, almost all of the TiO_2-HMSs precursor have totally transformed into urchin-like titanate nanosheets aggregation.

Based on the analysis mentioned above, we proposed the formation process for this unique hierarchical TiO_2-HMSs-NSs (Scheme 1). Firstly, when the precursor TiO_2-HMSs were exposed to basic solution, the Ti—O—Ti bonds in the TiO_2 nanoparticles of the precursor were broken to form Ti—O—Na [20]. Single- or multilayered titanate nanosheets were formed in inner and outer surface layer of the primary TiO_2-HMSs, and then these nanosheets converted into nanotubes, either by scrolling (rolling-up) single layer nanosheets or by curving (wrapping) of conjoined nanosheets. Why does the synthesized TiO_2-HMSs-NSs sample retain the original sphere morphology of TiO_2-HMSs precursor at first? This is because that both anatase and titanate contain zigzag ribbons of TiO_6 octahedra that share four edges with the others, and the common structural features make the phase transition from anatase to titanate relatively easy [22]. Therefore, the original hollow sphere morphology could be retained. After that, the interior of shell begins to contact with alkali solutions. Therefore, more titanium dioxide nanoparticles transformed into nanosheets or nanotubes. As the extension of hydrothermal time, the nanosheets or nanotubes gradually grow. At the same time, the inside diameters of primary TiO_2 hollow microspheres becomes smaller and smaller. At last, the hollow interior can hardly be observed. Nanosheets or nanotubes cross each other, forming hierarchical porous TiO_2-HMSs-NSs.

For comparison, we also prepared TiO_2 solid microspheres assembly from nanosheets (TiO_2-SMSs-NSs, S3 sample) by same strategy except using TiO_2-SMSs as precursor (Table 1). Comparing
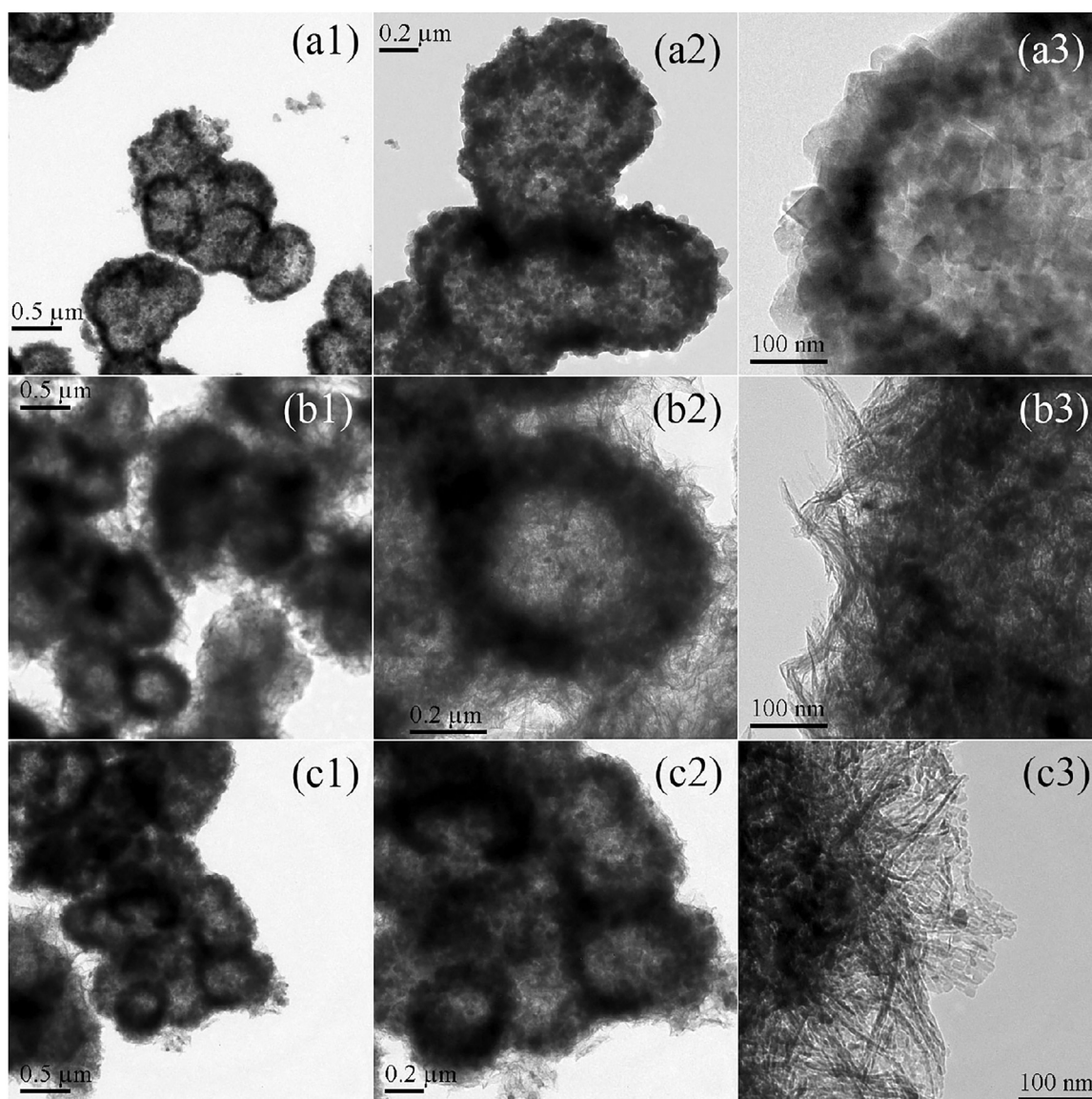
Fig. 1. TEM images of TiO₂-HMSs precursor (a), which were followed by hydrothermal treatment in NaOH solution and acid-wash before (b) and after (c) calcination to TiO₂-HMSs-NSs (H2 sampe), respectively.

Fig. 4e and f, it can be seen that S3 sample also appears urchin-like structure similar to TiO₂-HMSs-NSs sample (H3).

3.2. Nitrogen adsorption-desorption and UV–vis absorption

The BET surface area and pore structure of the hierarchical TiO₂-HMSs-NSs were further examined by nitrogen adsorption-desorption analysis. Fig. 5 compares the nitrogen adsorption-desorption isotherms TiO₂-HMSs precursor (H0), hierarchical TiO₂-HMSs-NSs (H3) and TiO₂-SMS-NSs (S3). It can be seen that the adsorption isotherms of H3 and S3 shift upward when compared with that of H0 sample, reflecting the enlarged BET surface areas of H3 and S3 sample. This is because that both the surface of H3 and S3 microspheres are covered with multi-layered TiO₂ nanosheets (Figs. 3 and 4). The isotherm curve of H3 can be categorized as an IUPAC type III adsorption isotherm, giving a specific surface area of $184 \, m^2 \, g^{-1}$, which is 8.76 and 2.52 times higher than precursor TiO₂-HMSs ($21 \, m^2 \, g^{-1}$) and the control S3 sample ($73 \, m^2 \, g^{-1}$), respectively (Table 1).
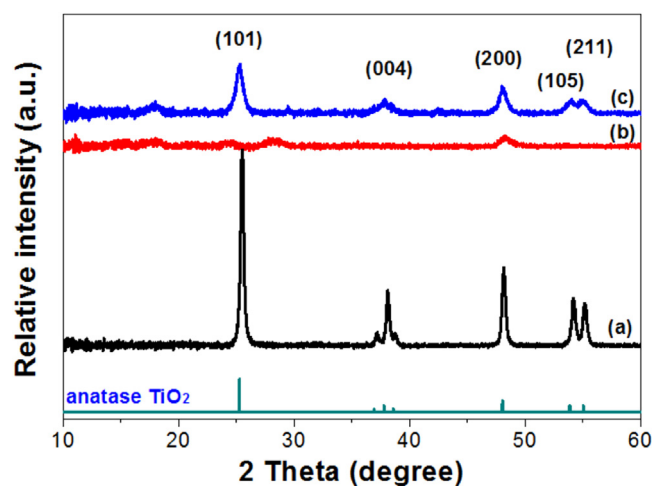

Fig. 2. XRD patterns of TiO₂-HMSs precursor (a), the resulted samples treated by hydrothermal treatment in NaOH solution for 2 h before (b) and after (C) calcination (H2 sample), respectively.
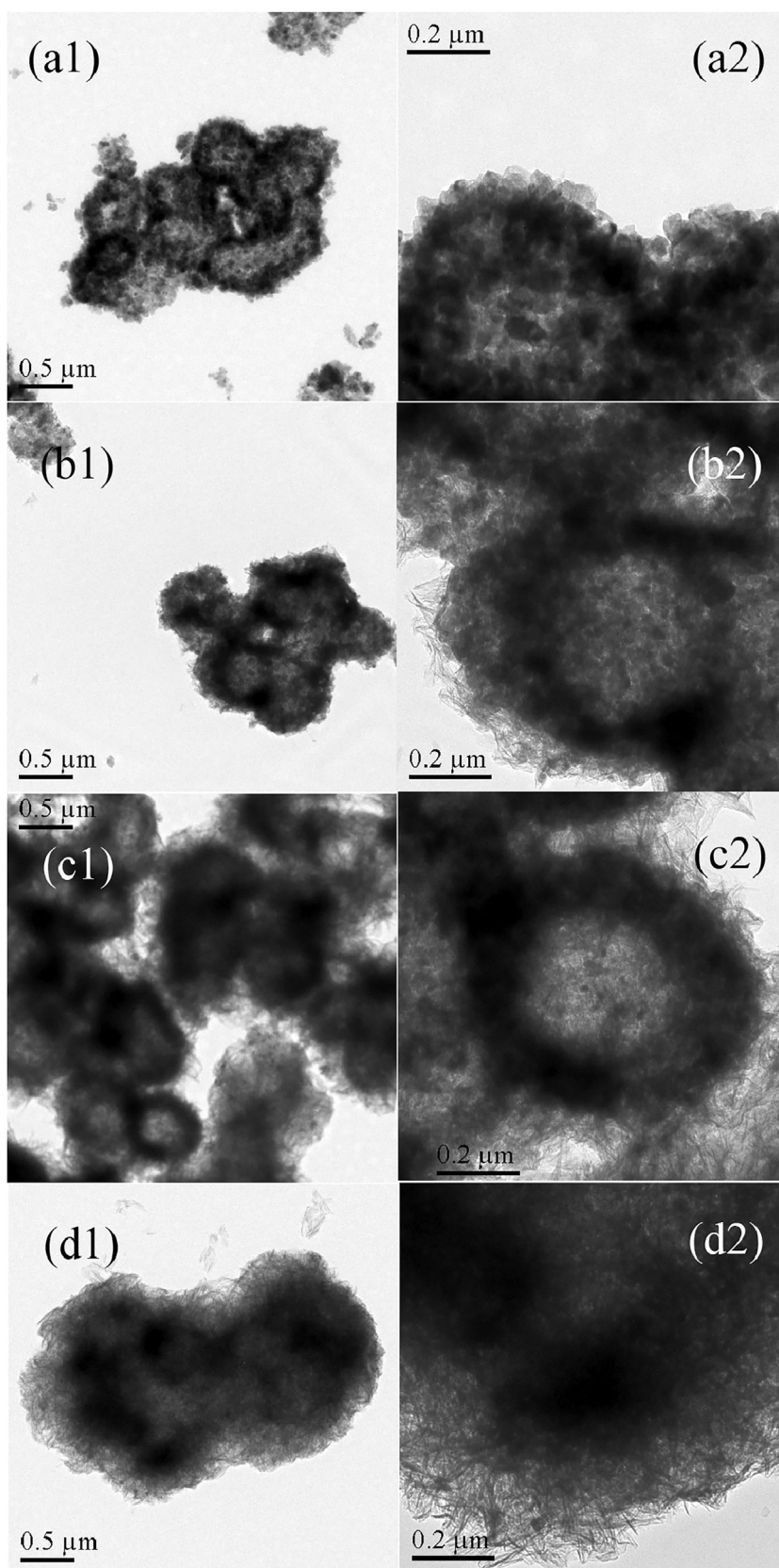
Fig. 3. TEM images of the samples after acid-wash, which were synthesized by hydrothermal treatment of the TiO_2-HMSs in basic solution for 1 h (a), 1.5 h (b), 2.5 h (c) and 3 h (d), respectively.
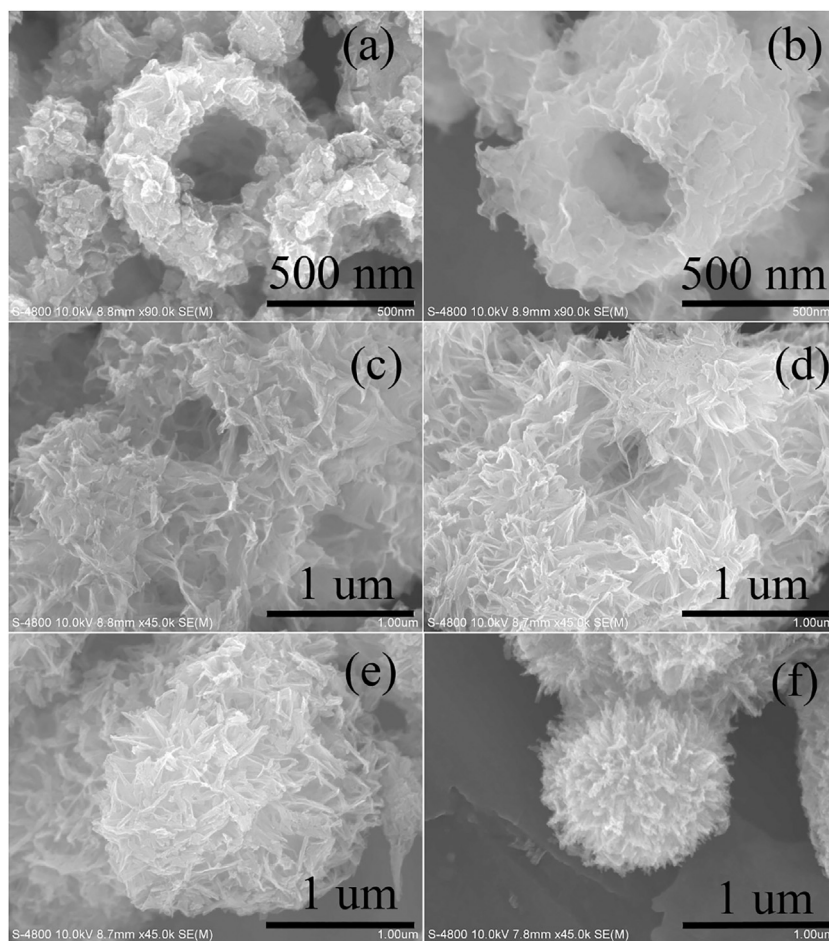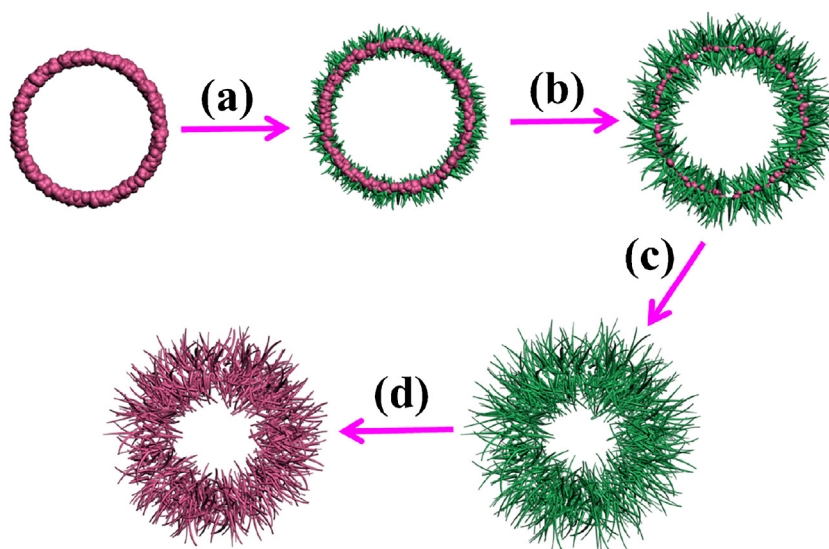
Fig. 4. SEM images of the photocatalysts recording the shape-evolution of the TiO$_2$-HMSs-NSs by hydrothermal treatment of TiO$_2$-HMSs precursor for 1 h (a), 1.5 h (b), 2 h (c), 2.5 h (d) and 3 h (e), respectively. TEM image of TiO$_2$-SMSs-NSs (S3) was shown in (f).

Scheme 1. Schematic diagram depicts the morphology evolution with reaction time to form hierarchical TiO$_2$-HMSs-NSs photocatalyst. Pink and green colours represent anatase TiO$_2$ and titanate, respectively. Steps a-c indicate the extension of hydrothermal reaction time, and step d represents phase transformation from titanate to anatase TiO$_2$ due to calcination. (For interpretation of the references to color in this figure legend, the reader is referred to the web version of this article.)

One hysteresis loop at a relative pressure range of 0.7–1.0 can be observed for H3 TiO$_2$-HMSs-NSs sample, and the shape of the hysteresis loop is of type H3, suggesting narrow slit-shaped pores that are generally associated with plate-like particles, which agrees well with their urchin-like morphology (Fig. 4e) [24]. Inset of Fig. 5 shows the pore size distribution curves of the photocatalysts. It can be seen that TiO$_2$-HMSs-NSs (H3 sample) possesses the largest pore volume (0.70 m^2 g^{-1}), which is 2 and 6.4 times higher
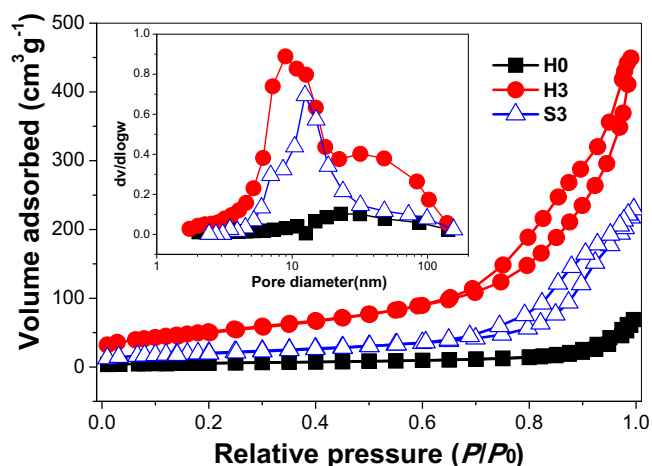
Fig. 5. Nitrogen adsorption-desorption isotherms and the corresponding pore size distributions (inset) of the TiO₂ samples for H0, H3 and S3, respectively.
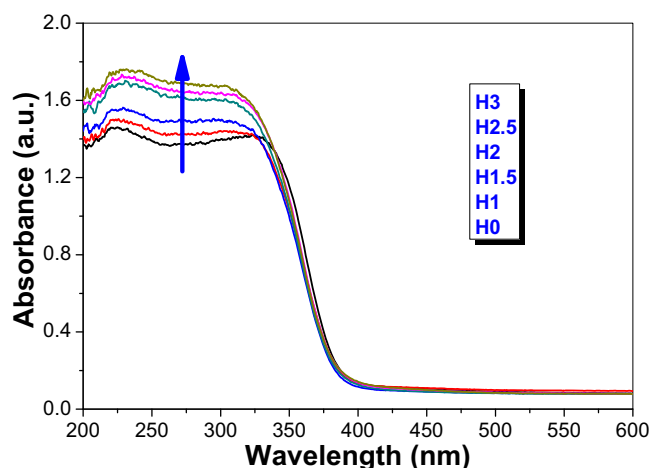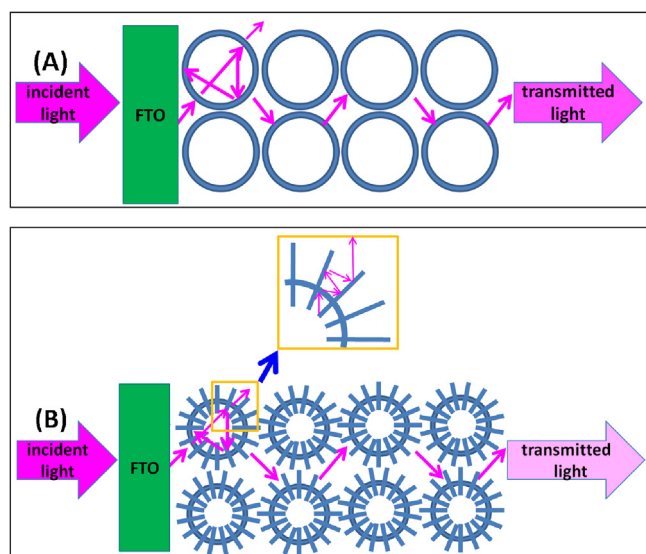

Fig. 6. UV–vis absorption spectra of TiO₂ photocatalysts.

Scheme 2. Schematic diagram showing the improved light-harvesting ability of TiO₂-HMSs-NSs film (B) than that of ordinary TiO₂-HMSs film (A) due to the multi-reflection of light within TiO₂ nanosheets that cover the surface of TiO₂-HMSs-NSs (inset).

Fig. 7. Comparison of the current–voltage characteristics of DSSCs.

Table 2
The photovoltaic parameters of the DSSCs.

Samples	I_{SC} (mA cm^{-2})	V_{OC} (V)	FF	η (%)
H0	7.51	0.719	0.694	3.75
H1	9.24	0.716	0.707	4.68
H1.5	10.1	0.75	0.689	5.22
H2	11.5	0.709	0.732	5.97
H2.5	9.86	0.715	0.729	5.14
H3	9.45	0.71	0.724	4.86
S3	10.7	0.701	0.598	4.49

than that of TiO₂-SMSs-NSs (0.36 m² g⁻¹) and TiO₂-HMSs precursor (0.11 m² g⁻¹), respectively. In addition, TiO₂-HMSs-NSs sample shows a typical bimodal mesopore size distribution.

From Table 1, it can be seen that both the BET surface area and pore volume of TiO₂-HMSs-NSs sample steadily increases with extension the reaction time. The enlarged BET surface area means the exposure of more active sites, and the improved pore volume, due to the formation of TiO₂ nanosheets on the surface of TiO₂ microspheres, allows multi-reflections of light within the interior cavity that facilitates more efficient use of the light source (Scheme 2). According to the UV–vis diffuse reflectance spectra, the absorption ability of the photocatalyst in UV region also increases with increasing the hydrothermal reaction time (Fig. 6). This is due to the good light-scattering property of the TiO₂ nanosheets on the surface of TiO₂-HMSs-NSs.
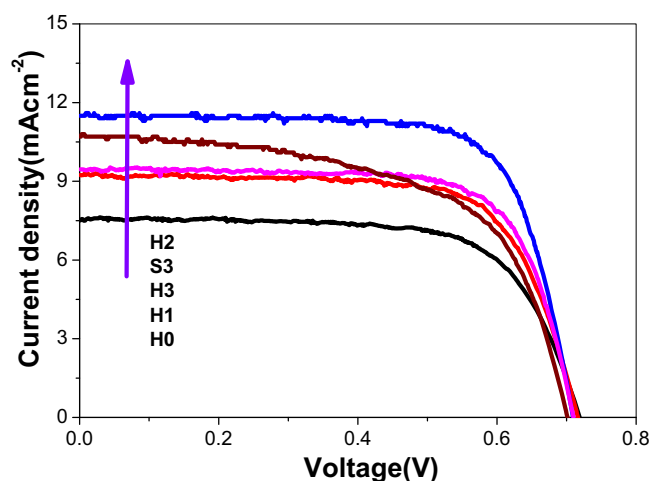
3.3. Photoelectric conversion efficiency in DSSCs

The photoelectric conversion efficiency (η) was calculated according to eqn (4):

$$\eta\,(\%) = \frac{V_{OC}I_{SC}FF}{P_{in}} \times 100 \qquad (4)$$

Where V_{OC}, I_{SC}, and FF are open circuit voltage, short circuit current density, and fill factor, respectively. P_{in} is the light energy of the incident monochromatic light. The comparison of the photovoltaic density-voltage (I–V) characteristics of TiO₂ DSSCs are illustrated in Fig. 7, and the corresponding photovoltaic parameters were summarized in Table 2. It can be observed that I_{SC} of the TiO₂-HMSs-NSs based film cell increases first and then decreases, and H2 film cell exhibits the highest I_{SC} (11.5 mA cm⁻²), which is 1.53 times higher
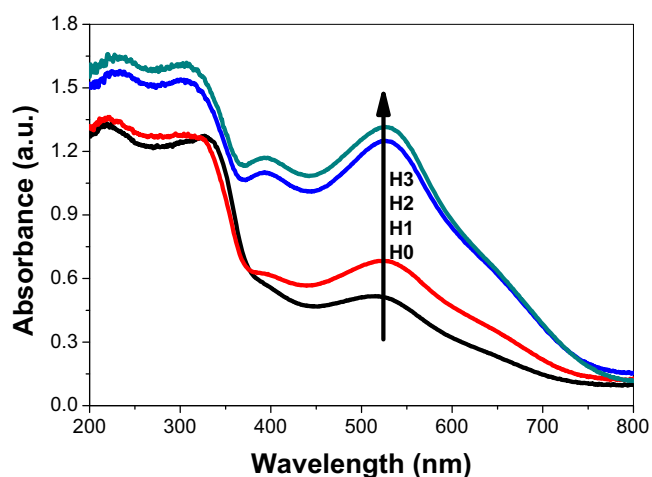
Fig. 8. Comparison of the UV–vis diffuse absorption spectra of film electrodes.

Fig. 9. Comparison of the Nyquist plots of DSSCs based on TiO₂-HMSs precursor (H0), TiO₂-HMSs-NSs (H2 and H3) and TiO₂-SMSs-NSs (S3) film electrode.

Table 3
Electron transport property during the photovoltaic process of DSSCs.

Sample	R_S (Ω)	R_C (Ω)	R_t (Ω)
H0	18.7	18.7	38.5
H2	13.7	7.6	22.1
H3	13.0	8.9	26.7
S3	18.9	15.9	21.4

than that of TiO₂-HMSs precursor film cell (7.51 mA cm⁻²). As the V_{OC} values of these cells are similar (0.7–0.75 V), H2 sample TiO₂-HMSs-NSs based film cell therefore shows the highest photoelectric conversion efficiency (5.97%), which is 1.59 times and 1.33 times higher than that of TiO₂-HMSs precursor (3.75%) and TiO₂-SMS-NSs (4.49%) based film cell, respectively.

Because TiO₂-HMSs-NSs can make a closer contact with FTO glass when compared with primary TiO₂-HMSs (Scheme 2), it is not hard to understand that TiO₂-HMSs-NSs film based DSSCs possess a higher *FF* (0.732 for H2 sample) than TiO₂-HMSs film based DSSCs (0.694 for H0 sample). However, if the size of TiO₂-NSs is too large, the deposition of TiO₂-HMSs-NSs over FTO glass will become loose, resulting in a smaller *FF* (0.724 for H3 sample). Therefore, it is reasonable that H2 sample TiO₂-HMSs-NSs based film cell shows the highest photoelectric conversion efficiency (5.97%) due to the good contact between TiO₂ and FTO glass.

UV–vis absorption spectra of TiO₂-HMSs-NSs was shown in Fig. 6. It can be seen that the absorption of the photocatalyst in UV region increases with increasing the reaction time, reflecting that TiO₂ nanosheets layer facilitate the multi-reflections of the light within TiO₂-HMSs-NSs (Scheme 2). Enlarged BET surface area also results in an increase in dye adsorption on the surface TiO₂-HMSs-NSs, which was confirmed by UV–vis absorption spectra of the film electrode after adsorption of sensitizer dye (Fig. 8). Therefore, when compared with that of TiO₂-HMSs precursor film cell, the reasons for the higher photoelectric conversion efficiency of hierarchical TiO₂-HMSs-NSs film cell can be summarized as follows:

(1) The pore volume of TiO₂-HMSs-NSs film is larger than that of TiO₂-HMSs precursor film, which can enhance transfer and diffusion of electrolyte (Table 1). It is well known that the efficient diffusion of I₃⁻/I⁻ to regenerate the dye is important to the photovoltaic response of the solar cells.
(2) Unique structure of TiO₂ nanosheets on the surface of TiO₂-HMSs-NSs causes multi-reflections of the light, extending the distance that light travels within the photoelectrode film and provides the photons with more opportunities to be absorbed by the dye molecules [25], resulting in a significant increase in the light harvesting capability of the photoelectrode (Fig. 6 and Scheme 2). The formation of TiO₂-NSs make a good contact between TiO₂-HMSs-NSs and FTO glass, resulting in a high *FF*, therefore improving the photoelectric conversion efficiency (Scheme 2 and Eq. (4)).
(3) Improved sensitization dye adsorption property due to the enlarged BET surface area of the hierarchical TiO₂-HMSs-NSs (Fig. 8 and Table 1) means that more photo-generated elec-
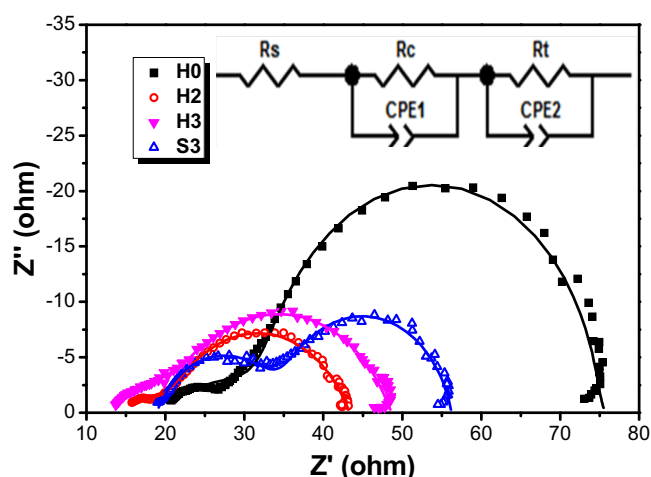
trons can be injected into the conduction band of anodic TiO₂ electrode, increasing the photocurrent I_{SC} (Fig. 7).

When compared with that of primary TiO₂-HMSs precursor (H0), the BET surface area of H2 TiO-HMSs-NSs improved 7.3 times. However, the photoelectric conversion efficiency of H2 film based DSSCs is only 1.6 times higher than that of H0 film based DSSCs. This infers that, the effect of BET surface area on photoelectric conversion of DSSCs is not so obvious than on photocatalytic degradation. To further understand the effect of film structure on the photovoltaic performance of DSSCs, the electrochemical impedance spectroscopy (EIS) measurements were performed to reveal the electron transport during the photovoltaic process of DSSCs. Fig. 9 compares the Nyquist plots of the DSSCs based on TiO₂-HMSs precursor (H0), TiO₂-HMSs-NSs (H2 and H3) and TiO₂-SMSs-NSs (S3) film electrodes. Two semicircles including a small one at high frequency and a large one at middle frequency can be observed. The Nyquist plots were modeled with an equivalent circuit (inset in Fig. 9) using non-linear-least-square fit analysis software (Zview software). R_S is attributed to the sheet resistance of the FTO glass substrate and the contact resistance at the FTO/TiO₂ interface. The R_S values of DSSCs based on H0, H2, H3 and S3 electrodes calculated according to the equivalent circuit were 18.7, 13.7, 13.0 and 18.9 Ω (Table 3), respectively. It is can be clearly seen that the hierarchical TiO₂-HMSs-NSs have smaller R_S when compared with priminary TiO₂-HMSs and counterpart TiO₂-SMSs-NSs, implying better electronic contact between TiO₂-HMSs-NSs and FTO glass (Scheme 2).

The small semicircle in the high frequency region is related to the charge transfer resistance (R_C) and interfacial capacitance (CPE1) at the interfaces between the electrolyte and Pt electrode, and the large semicircle in the middle frequency region is related to the electron transport resistance (R_t) within the TiO₂ film and interfacial capacitance (CPE2) at the TiO₂/dye/electrolyte interface[3,17]. Similarly, H2 TiO₂-HMSs-NSs based film cell possesses relatively smaller values of R_C and R_t, therefore it is not hard
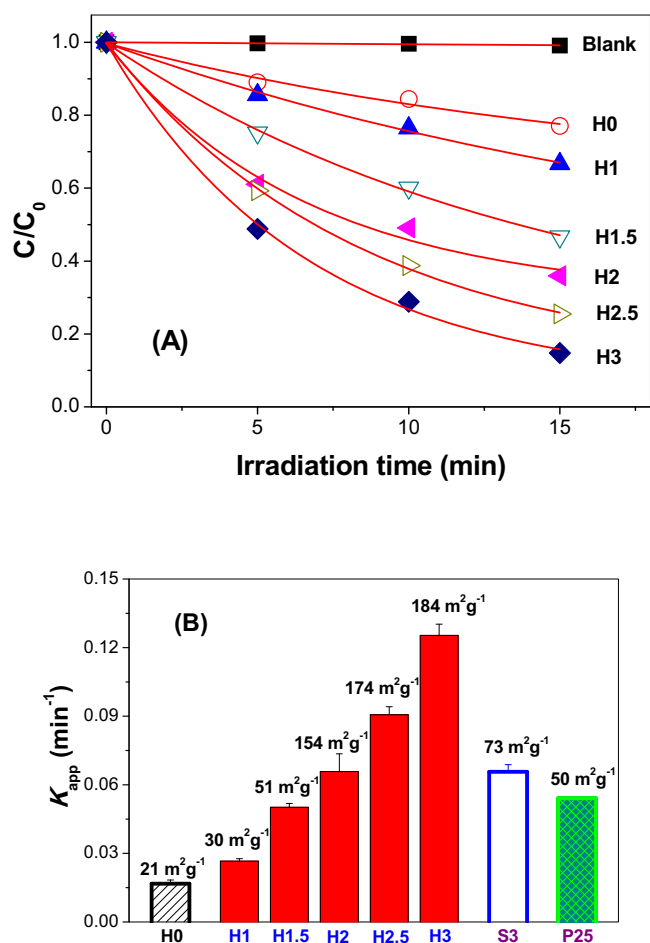
Fig. 10. Photocatalytic degradation profiles of X3B in TiO_2 suspensions under UV irradiation (A) and comparison of the degradation rate constants (B).

to understand that TiO_2-HMSs-NSs based film photoanode exhibits a better photovoltaic performance in DSSCs.

3.4. Photocatalytic degradation

The photocatalytic activity of the photocatalyst was also evaluated using X3B, an anionic azo dye, as probe molecule under UV irradiation. In the absence of any photocatalyst, X3B shows little degradation under irradiation, reflecting the high stability of the dye (Fig. 10A) [13]. However, obvious degradation was observed in the presence of TiO_2 photocatalyst, and the degradation profile obeys a pseudo-first-order reaction rate equation in kinetics. Therefore, the apparent degradation rate constant, K_{app}, was used to compare the relative photoreactivity of the photocatalyst. As shown in Fig. 10B, the photoreactivity of the hierarchical TiO_2-HMSs-NSs was found to steadily increase with increasing the hydrothermal reaction time that used in preparation the photocatalyst. The rate constant for H3 TiO_2-HMSs-NSs sample is as higher as $0.125\,min^{-1}$, exceeding TiO_2-HMSs precursor ($0.0167\,min^{-1}$), counterpart photocatalyst TiO_2-SMSs-NSs ($0.0657\,min^{-1}$) and commercial P25 TiO_2 ($0.0542\,min^{-1}$) by a factor of 7.5, 1.9 and 2.3, respectively.

It is often observed that the photocatalytic activity of TiO_2 is a function of physical parameters such as the crystalline phase, crystallinity, average crystallite size, pore size, pore volume and specific surface area, and so on [26]. Since the surface area of TiO_2-HMSs-NSs steady increases with increasing the hydrothermal reaction time (Table 1), it is not hard to understand the positive relation-

ship between photoreactivity of hierarchical TiO_2-HMSs-NSs and their BET surface area (Fig. 10B).

Although the crystallinity of TiO_2-HMSs-NSs is much poorer than that of primary TiO_2-HMSs (Fig. 2), the photocatalytic activity of TiO_2-HMSs-NSs was greatly enhanced, exhibiting the BET surface area-dependent photocatalytic activity (Fig. 10). The H3 samples showed best performance in degradation of dye, which is different from the case of DSSC. This reflects that, not only the BET surface areas, but also other factors such as pore structure and the contact between photocatalyst and FTO glass can affect the electron transportation behaviour, influencing the photoelectric conversion efficiency of DSSCs

Please note that the BET surface area of H3 sample is as high as $184\,m^2\,g^{-1}$, which is 3.7 times higher than that of P25 TiO_2 ($50\,m^2\,g^{-1}$). When compared with TiO_2 nanoparticles such as commercial P25 TiO_2, this unique hierarchical TiO_2-HMSs-NSs has the merits of being higher photoreactivity and easy to recycle, indicating that it is promising to be widely used in practical applications.

4. Conclusions

Unique hierarchical TiO_2 hollow microspheres assembly from nanosheets (TiO_2-HMSs-NSs) were synthesized by hydrothermal treatment of the primary TiO_2-HMSs. Both the BET surface areas and photoreactivity of TiO_2-HMSs-NSs are positively related to the hydrothermal reaction time. The photoelectric conversion efficiency of TiO_2-HMSs-NSs based film DSSCs is as high as 5.97%, much higher than that of precursor TiO_2 hollow microspheres (TiO_2-HMSs) and counterpart TiO_2 solid microspheres assembly from nanosheets (TiO_2-SMSs-NSs) based film DSSCs. The promoted performance of TiO_2-SMSs-NSs is ascribed to the synergistic effects of good contact between TiO_2 and FTO glass, improve pore volume, increased BET surface area and enhanced light scattering. The preparation of the high efficient TiO_2-SMSs-NSs based film photoanode has the merit of being simple and easy to control. The present study is also of great interest in photocatalysis, catalysis, separation and purification and so on.

Acknowledgments

References

[1] H.M. Zhang, Y.H. Han, X.L. Liu, P.R. Liu, H. Yu, S.Q. Zhang, X.D. Yao, H.J. Zhao, Chem. Commun. 46 (2010) 8395–8397.
[2] A. Hegazy, N. Kinadjian, B. Sadeghimakki, S. Sivoththaman, N.K. Allam, E. Prouzet, Solar Energy Mater. Sol. Cells 153 (2016) 108–116.
[3] J.G. Yu, J.J. Fan, K.L. Lv, Nanoscale 2 (2010) 2144–2149.
[4] Y. Ide, N. Inami, H. Hattori, K. Saito, M. Sohmiya, N. Tsunoji, K. Komaguchi, T. Sano, Y. Bando, D. Golberg, Y. Sugahara, Angew. Chem. Int. Ed. 55 (2016) 3600–3605.
[5] W.G. Wang, H.Y. Zhang, R. Wang, M. Feng, Y.M. Chen, Nanoscale 6 (2014) 2390–2396.
[6] K.L. Lv, J.G. Yu, J.J. Fan, M. Jaroniec, CrystEngComm 14 (2011) 7044–7048.
[7] M. Mollavali, C. Falamaki, S. Rohani, Int. J. Hydrogen Energy 40 (2015) 12239–12252.
[8] X.R. Cao, G.H. Tian, Y.J. Chen, J. Zhou, W. Zhou, C.G. Tian, H.G. Fu, J. Mater. Chem. A 2 (2014) 4366–4374.
[9] E. Formo, E. Lee, D. Campbell, Y. Xia, Nano Lett. 8 (2008) 668–672.
[10] N.Q. Wu, J. Wang, D.N. Tafen, H. Wang, J. Guo Zheng, J.P. Lewis, X.G. Liu, S.S. Leonard, A. Manivannan, J. Am. Chem. Soc. 132 (2010) 6679–6685.
[11] X.G. Han, Q. Kuang, M.S. Jin, Z.X. Xie, L.S. Zheng, J. Am. Chem. Soc. 131 (2009) 3152–3153.
[12] J.F. Lan, X.F. Wu, K.L. Lv, L.L. Si, K.J. Deng, Chin. J. Catal. 36 (2015) 2237–2243.

[13] L.L. Si, Z.A. Huang, K.L. Lv, H.P. Ye, K.J. Deng, Y.Y. Wu, J. Alloys Compd. 612 (2014) 69–73.

[14] G.T. Dai, L. Zhao, J. Li, L. Wan, F. Hu, Z.X. Xu, B.H. Dong, H.B. Lu, S.M. Wang, J.G. Yu, J. Colloid Interfaces Sci. 365 (2012) 46–52.

[15] J.H. Hu, S.W. Hu, Y.P. Yang, S.Q. Tong, J.J. Cheng, M.W. Chen, L. Zhao, J.X. Duan, Int. J. Photoenergy 2016 (2016) 4651654.

[16] J.H. Hu, L. Zhao, Y.P. Yang, H. Liao, S.M. Wang, X.D. Sun, J.J. Cheng, B.H. Dong, Int. J. Photoenergy 2014 (2014), Article ID 602692.

[17] J.H. Hu, J.J. Cheng, S.Q. Tong, L. Zhao, J.X. Duan, Y.P. Yang, J. Mater. Sci.: Mater. Electron. 27 (2016) 5362–5370.

[18] T. Marimuthu, N. Anandhan, R. Thangamuthu, S. Surya, J. Alloys Compd. 693 (2017) 1011–1019.

[19] Y. Zheng, J.H. Cai, K.L. Lv, J. Sun, H.P. Ye, M. Li, Appl. Catal. B 147 (2014) 789–795.

[20] Z.K. Zheng, B.B. Huang, X.Y. Qin, X.Y. Zhang, Y. Dai, Chem. Eur. J. 16 (2010) 11266–11270.

[21] Y. Liu, Y.F. Luo, A.A. Elzatahry, W. Luo, R.C. Che, J.W. Fan, K. Lan, A.M. Al-Enizi, Z.K. Sun, B. Li, Z.W. Liu, D.K. Shen, Y. Ling, C. Wang, J.X. Wang, W.J. Gao, C. Yao, K.P. Yuan, H.S. Peng, Y. Tang, Y.H. Deng, G.F. Zheng, G. Zhou, D.Y. Zhao, ACS Cent. Sci. 1 (2015) 400–408.

[22] H.Y. Zhu, Y. Lan, X.P. Gao, S.P. Ringer, Z.F. Zheng, D.Y. Song, J.C. Zhao, J. Am. Chem. Soc. 127 (2005) 6730–6736.

[23] J. Sun, X. Yan, K.L. Lv, S. Sun, K.J. Deng, D.Y. Du, J. Mol. Catal. A 367 (2013) 31–37.

[24] K.L. Lv, Q.J. Xiang, J.G. Yu, Appl. Catal. B 104 (2011) 275–281.

[25] H.X. Li, Z.F. Bian, J. Zhu, D.Q. Zhang, G.S. Li, Y.N. Huo, H. Li, Y.F. Lu, J. Am. Chem. Soc. 129 (2007) 8406–8407.

[26] Y.M. Xu, K.L. Lv, Z.G. Xiong, W.H. Leng, W.P. Du, D. Liu, X.J. Xue, J. Phys. Chem. C 111 (2007) 19024–19032.